Process Parameters Optimization for Thin-walled Tube Push-bending Using Response Surface Methodology

Wenlong Xie
Institute of Metal Research Chinese Academy of Sciences
Weihao Jiang
Technical University of Cluj-Napoca
Yunfeng Wu
Technical University of Cluj-Napoca
Hongwu Song (hwsong@imr.ac.cn)
Institute of Metal Research Chinese Academy of Sciences https://orcid.org/0000-0003-4872-6807
Siying Deng
Institute of Metal Research Chinese Academy of Sciences
Lucian Lăzărescu
Institute of Metal Research Chinese Academy of Sciences
Shihong Zhang
Technical University of Cluj-Napoca
Dorel Banabic
Technical University of Cluj-Napoca

Research Article

Keywords: Thin-walled tube, Push-bending, Process optimization, Response surface methodology

Posted Date: March 8th, 2021

DOI: https://doi.org/10.21203/rs.3.rs-277097/v1

Version of Record: A version of this preprint was published at The International Journal of Advanced Manufacturing Technology on October 19th, 2021. See the published version at https://doi.org/10.1007/s00170-021-08196-8.

Process parameters optimization for thin-walled tube push-bending using response surface methodology

Wenlong Xie[1,2], Weihao Jiang[3], Yunfeng Wu[4], Hongwu Song[1,*], Siying Deng[1], Lucian Lăzărescu[5], Shihong Zhang[1], Dorel Banabic[5]

[1] *Shi-changxu Innovation Center for Advanced Materials, Institute of Metal Research, Chinese Academy of Sciences, Shenyang 110016, China*

[2] *School of Materials Science and Engineering, University of Science and Technology of China, Shenyang 110016, China*

[3] *Guizhou Liyang Aero-Engine Corporation, Guiyang 550000, China*

[4] *Beijing Institute of Astronautical Systems Engineering, Beijing 100076, China*

[5] *Department of Manufacturing Engineering, Technical University of Cluj-Napoca, Cluj-Napoca 400641, Romania*

***Corresponding author.**

Phone: +86-24-83970203

Email: hwsong@imr.ac.cn

Acknowledgements

The authors appreciate the supports from the National Natural Science Foundation of China, China (Grant No: 51875547).

Abstract

In this paper, the response surface methodology (RSM) and finite element (FE) simulation were applied to optimize the push-bending process parameters of the thin-walled tube with polyurethane mandrel. The objective of the present work is to predict the optimal set of process parameters including the relative length of the mandrel (L/D), the friction coefficient between die and tube (μ_1), the friction coefficient between polyurethane and tube (μ_2) and Poisson's ratio of polyurethane (υ) to obtain qualified bent tubes. Three empirical models were developed to describe the relationship between process parameters and quality parameters of the bent tubes. In addition, the significant factors affecting the forming quality were analyzed using analysis of variance (ANOVA) of each model. Response surfaces were constructed to study the effect of each process parameter on the quality of the bent tubes. Finally, the process optimization window with the maximum thinning rate (φ) less than 20%, the maximum thickening rate (ψ) less than 17%, and the maximum cross-section ovality (ξ) less than 5% of the bent tube was established. Qualified bent tubes with diameter of 144 mm, wall thickness of 2 mm, and bending radius of 280 mm were formed experimentally by following the established process window.

Keywords: Thin-walled tube; Push-bending; Process optimization; Response surface methodology

1 Introduction

With the development of modern industry, light-weighting has become more and more an urgent requirement and development direction of parts manufacturing, and large diameter thin-walled bent tubes are widely used in the aerospace, aviation, ships, oil industries as the typical lightweight parts [1,2]. There are four main defects in the tube bending, including over thinning of the outer wall of the bent tube, wrinkling in the inner wall, cross-sectional distortion and spring back after unloading [3-5]. Especially as the relative wall thickness (t_0/D; D, initial outer diameter; t_0, initial wall thickness) decrease, more serious forming defects will occur. Most tube bending processes are dedicated to reducing even avoiding the generation of the above defects. Many scholars have carried out researches on solving the problems in the tube bending process by using different bending methods such as NC bending [6], press bending with hydraulic pressure [7] and push-bending [8], etc.

No matter which kind of tube bending technology is adopted, the appropriate process parameters play a vital role in the bending forming quality of the tube. Therefore, the optimization of process parameters must be considered in the actual bending process. By optimizing the process parameters, the potential of the tube bending technology can be fully developed. The forming quality of the tube is affected by the interaction of multiple forming parameters. Empirical or trial-and-error methods are still the most commonly used in actual production, which can no longer meet the production of high-quality large-diameter thin-walled elbow tubes.

Nguyen D T et al. [9] selected mandrel diameter, the distance between mandrel rings, and distance from the tip of the mandrel bar to the center of the base die to study their effects on the bending quality of copper JIS25A according to Taguchi's orthogonal array and finite element simulation. R. Safdarian [10] studied the effect of pressure of pressure die, boosting velocity of pressure die, friction between the tube and pressure die, mandrel position and number of mandrel balls in rotary draw bending on the fracture, wrinkling and tube's ovality of BS 3059 steel tube. Xu et al. [11,12] optimized the parameters such as polyurethane length and friction coefficient in the push-bending process using sectional elastomers as mandrel, and the 1Cr18Ni9 and 5A02 tubes were well-formed. To realize the control of spring back and section deformation, the multi-parameter sensitivity analysis method was used to obtain the processing parameters in the bending process of rectangular tubes [13]. Li et al. [14] provided a comprehensive diagram of tube bending limits during rotary draw bending in a range of tube sizes, material types and processing parameters, and experimental verification was also carried out by several practical bending schemes. Lăzărescu [15] adopted Finite Element Simulation and Response Surface Methodology to optimize the tube bending process (relative bending radius (R/D) and relative tube diameter (D/t)) and the relationship between the cross section ovality and wall thinning. And the statistical models were used to establish an optimal technological window for the tube bending process in order to obtain products with an acceptable quality.

Some advanced optimization methods have been used to obtain useful regularities from the data, which will be of great value in guiding production. The response surface method (RSM) has been widely used in multi-target process parameter optimization. And the RSM can be used to predict the empirical functions between variables and responses and to find the optimal combination of variables. By using RSM and FEM, Lin et al. [16] developed the empirical equation to explore the relationship

between the principal strain of fracture risk elements and the working parameters, and the model adequacy was checked and confirmed using analysis of variance (ANOVA). Lepadatu et al. [17] carried out the optimization of spring back in sheet metal bending processes using FEM and RSM. Liu et al. [18] used the RSM to research the influences of three experimental factors on maximum forming load and maximum tool wear depth, and the optimal parameter combination was employed to redesign the billet and the forging tools for industrial practice.

A modified thin-walled tube push-bending process with polyurethane mandrel has been proven to be suitable for forming large diameter and thin-walled tubes [19]. In this paper, the process parameters were optimized and the potential of this tube bending process can be fully developed. The Central Composite Design (CCD), one method of RSM, is introduced and adopted to develop three empirical equations based on numerical FE simulation results to describe the relationship between quality characteristics and process parameters. Three bent tube quality characteristics, including the maximum thinning rate (φ), the maximum thickening rate (ψ) and the maximum cross-section ovality (ξ) were set as responses in RSM. The relative length of the mandrel (L/D), coefficient of friction between die and tube (μ_1), the coefficient of friction between polyurethane and tube (μ_2) and the Poisson's ratio of polyurethane (υ) were four factors in RSM. The empirical models were used in order to establish a technological window for the optimal tube bending. Finally, the reliability of the empirical equations is verified by experiments.

2 Experimental procedure and methods

2.1 Forming process

The schematic diagram of thin-walled tube push-bending process with polyurethane mandrel is illustrated in Fig. 1[19]. Prior to forming, a tubular blank filled with polyurethane mandrel of length L is inserted into a guide die. It should be noted that a metal thick plate stopper is welded on the front end of the tube blank to seal the polyurethane mandrel. During tube bending, the punch applies a pushing force on the back end of polyurethane mandrel and then under the common constraint of the guide, polyurethane mandrel and the bending die, the bent tube with bending radius of R is formed.

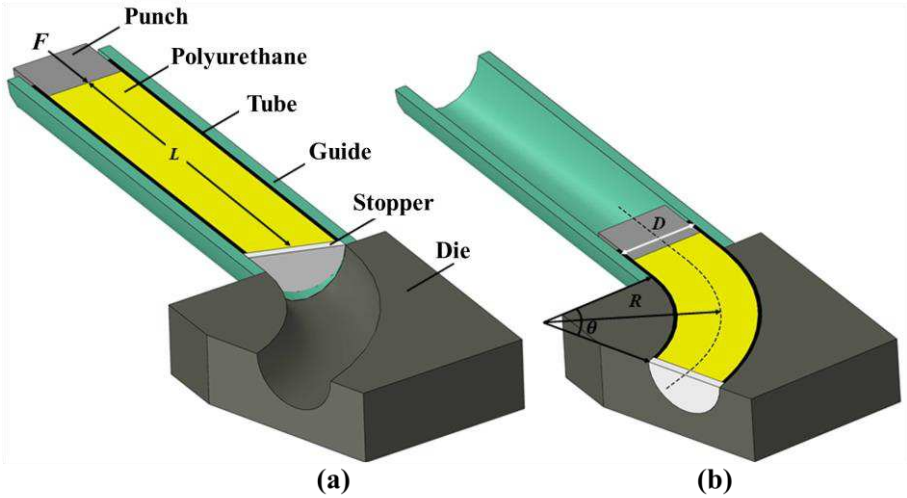

Fig.1 Schematics of the tube push-bending process with polyurethane mandrel (a) before bending (b) after bending [19].

From Fig. 2, the outer wall of the bent tube was thinned due to axial tensile stress while thickening even wrinkling appears in the inner wall due to axial compressive stress during tube bending. At the same time, the outer side wall of the elbow also moves inward causing cross-sectional distortion. In order to describe the above three defects, the maximum thinning rate φ, the maximum thickening rate ψ and the maximum cross-section ovality ξ are defined as:

$$\varphi = \frac{t_0 - t_{min}}{t_0} \tag{1}$$

$$\psi = \frac{t_{max} - t_0}{t_0} \tag{2}$$

$$\xi = \frac{D - D_{min}}{D} \tag{3}$$

where, t_0 is the initial tube wall thickness, t_{min} is the minimum wall thickness of bent tube after bending, t_{max} is the maximum wall thickness of bent tube after bending, D is the initial outer diameter of tube, and D_{min} is the minimum outer diameter of bent tube after bending.

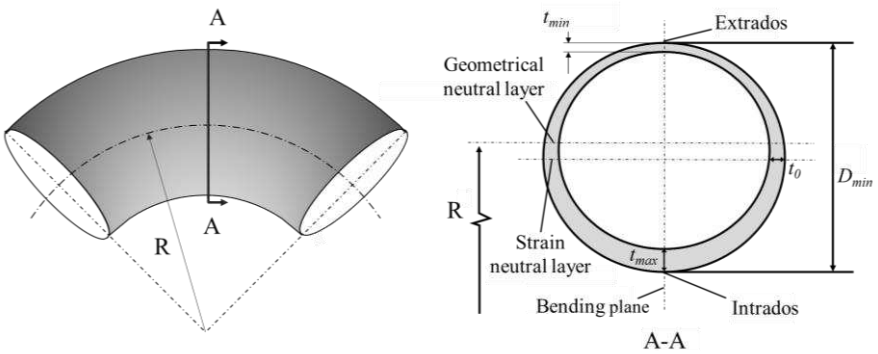

Fig.2 Schematic diagram of tube cross-section after bending.

The values of the above three defects will be used as the following optimization evaluation indicators, and the purpose of the optimization is to reduce the values of these three defects as much as possible.

2.2 Finite element modeling

As shown in Fig. 3, the 3D elastic–plastic FE model of the thin-walled tube push-bending process with polyurethane mandrel was built including the punch, polyurethane mandrel, tube, stopper, and die (including guide). The diameter of the tube is 144 mm and the wall thickness is 2 mm. The bending radius is 280 mm, and the bending angle is 70 °. Numerical simulations were carried out using ABAQUS/Explicit. Due to symmetry, only a half FE model was adopted to reduce the computational time. The die, punch and stopper were predefined as discrete rigid. The contacts at the tube-polyurethane and tube-die were modeled using surface-to surface contact algorithm. The friction behavior in the FE model was described with the classic Coulomb friction model. The tube was meshed by four-node doubly curved thin shell S4R with 5 integral points along the thickness direction. It is assumed that the material used in the simulation is a homogeneity, isotropic material following the Von-Mises yield criterion, and has anisotropic work hardening. The mechanical properties of 0Cr18Ni9 stainless steel tube blank were obtained by uniaxial tensile test of the specimens cut along the longitudinal direction of the tube, as shown in Fig. 4. The mechanical properties of 0Cr18Ni9 stainless steel tube blank are presented in Table 1 and its true stress-strain curve at room temperature is shown in Fig. 4.

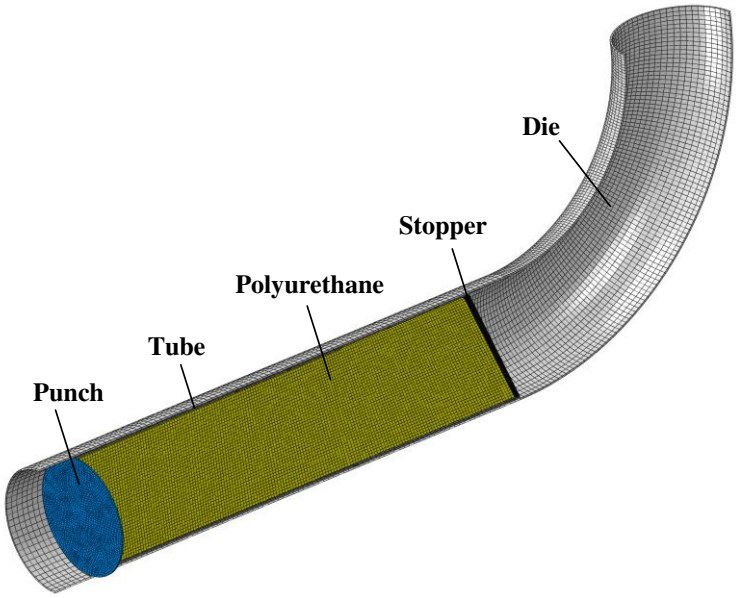

Fig. 3 Schematics of FE model.

Table 1 Mechanical properties of 0Cr18Ni9 tubular blank

Young's modulus E （MPa）	Density (kg/m^3)	Elongation （%）	Tensile yield strength （MPa）	Poisson's ratio
201000	7930	55	205	0.3

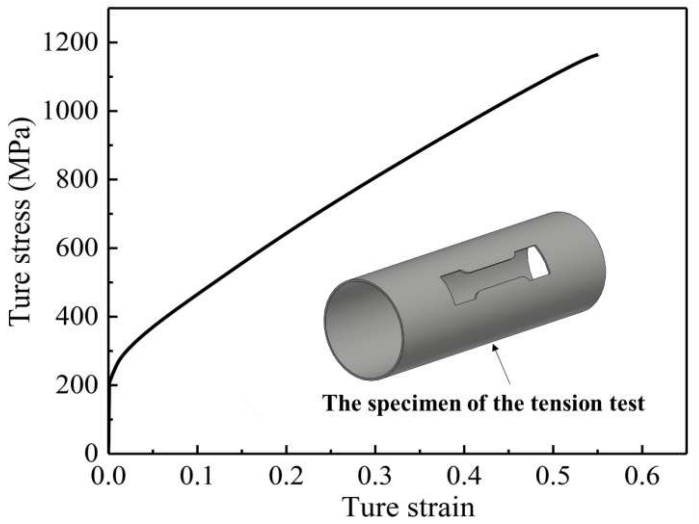

Fig. 4 True stress-strain curve of 0Cr18Ni9 tubular blank.

The Marlow strain energy potential model [19] was adopted in ABAQUS to characterize the mechanical properties of polyurethane mandrel, where only one set of test data (uniaxial, equibiaxial, or planar test data) is required. The relevant material performance testing experiments and results are shown in Fig. 5, and uniaxial compression and triaxial compression tests were carried out on polyurethane respectively. The elastic modulus E of polyurethane was 21 MPa by linear fitting of uniaxial compression test results (Fig. 5a). Meanwhile, the uniaxial compression results were also input into ABAQUS to establish the Marlow strain energy potential model. The polyurethane was put into a rigid capsule for triaxial compression tests. Due to the gap between polyurethane and rigid capsule, the polyurethane fully filled the capsule cavity after the filling stage and transition stage, and its stress state becomes three-dimensional compressive stress (Fig. 5a). And the compression modulus E_s of polyurethane was 2088 MPa by linear fitting of triaxial compression tests. Finally, Equation (4) was used to calculate the Poisson's ratio of polyurethane. The result of Poisson's ratio υ of polyurethane is 0.4983, which will be used in the Marlow strain energy potential model. The specific derivation process of Equation (4) can refer to our previous research [19]. It is worth noting that the experimental verification of the finite element model was also carried out to ensure the reliability of the model.

$$\upsilon = \frac{\sqrt{(E_s - E)^2 + 8E_s(E_s - E)} - (E_s - E)}{4E_s} \tag{4}$$

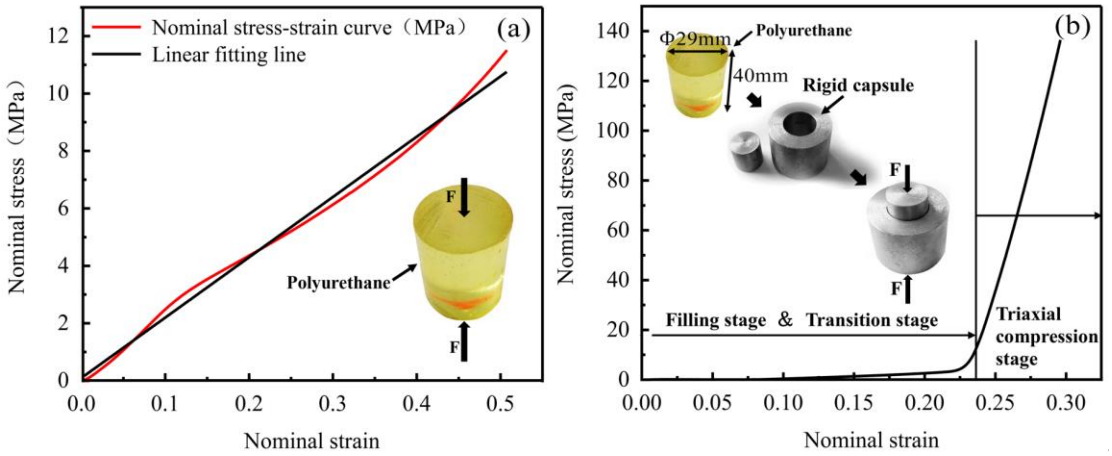

Fig. 5 Nominal stress-strain curve of polyurethane (a) Uniaxial compression (b) Triaxial compression [19].

2.3 Response surface methodology (RSM)

Response Surface Method is a statistical and mathematical method that processes the data by using regression analysis [20]. The empirical functions between response variables and processing parameters can be established by regression surface fitting. This empirical function can usually be obtained by fitting the experimental data using a first-order model or a second-order model.

The first-order model and the second-order model are shown in Equation (5) and Equation (6), respectively.

$$y = \beta_0 + \sum_{i=1}^{k} \beta_i x_i + \epsilon \tag{5}$$

$$y = \beta_0 + \sum_{j=1}^{k} \beta_j x_j + \sum_{i<j}^{k} \beta_{ij} x_i x_j + \sum_{j=1}^{k} \beta_{ij} x_j^2 + \epsilon \tag{6}$$

where, y is the response, x_i is the process parameters, ϵ is the experimental random error, $x_i x_j$ is the interaction term between parameter i and parameter j, x_j^2 is the secondary term of parameter j, and k is the number of process parameters. The constant terms and coefficients in models can be obtained by fitting the experimental data by the least square method, and then the empirical function between the response and each process parameter is established. The reliability of the response model can be tested by analysis of variance (ANOVA).

For process optimization, experimental design is very important, and reasonable experimental design can ensure the accuracy of experimental results while minimizing the number of experiments. In RSM, central composite design (CCD) is a popular experimental design method shown in Fig. 6. The CCD contains an imbedded factorial

or fractional factorial design with center points which is augmented with a group of "star points" that allow estimation of curvature. If the distance from the center of the design space to a factorial point is ±1 unit for each factor, the distance from the center of the design space to a star point is $|\alpha| > 1$.The value of α, in case of three factors is 1.682 [20].

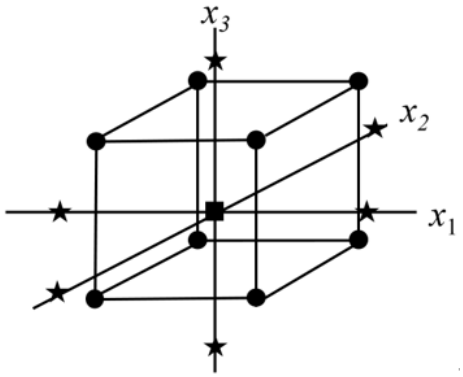

Fig.6 Central composite design for three factors

The central composite design response surface methodology (CCD-RSM) was used to optimization the push-bending with polyurethane mandrel process parameters in statistical modeling software Design Expert [15]. And the purpose of the integral bending forming of the seamless 0Cr18Ni9 stainless steel bent tube with outer diameter of 144 mm, wall thickness of 2 mm, bending radius of 280 mm, and bending angle of 70 ° was finally achieved.

The relative length of the mandrel (*L*/*D*), coefficient of friction between die and tube (μ_1), coefficient of friction between polyurethane and tube (μ_2) and Poisson's ratio of polyurethane (υ) are considered to be the main factors affecting the forming quality of the bent tube. And the forming quality of the bent tube is mainly described by the maximum thinning rate (φ), the maximum thickening rate (ψ) and the maximum cross-section ovality (ξ). Therefore, φ, ψ and ξ were selected as the responses in this study.

The range and levels of experimental variables investigated in this study are presented in Table 2. The experimental plan for the coded values in Table 2 and corresponding response values form FE simulations are shown in Table 3. The relative length of the mandrel (*L*/*D*), coefficient of friction between die and tube (μ_1), coefficient of friction between polyurethane and tube (μ_2) and Poisson's ratio of polyurethane (υ) are expressed by x_1, x_2, x_3 and x_4, respectively, for the convenience of expression. A zero value of the coefficient of friction for x_2 and x_3

could not be reached in practice, being the ideal case.

Table 2 Independent variables and level values

Independent variables	Symbol	Coded values (α= 1.682)				
		$-\alpha$	-1	0	+1	$+\alpha$
The relative length of the mandrel (L/D)	x_1	2.9	3.425	3.95	4.475	5
Coefficient of friction between die and tube (μ_1)	x_2	0	0.03	0.06	0.09	0.12
Coefficient of friction between polyurethane and tube (μ_2)	x_3	0.06	0.12	0.18	0.24	0.3
Poisson's ratio of polyurethane (υ)	x_4	0.49	0.4921	0.4942	0.4962	0.4983

3 Results and discussion

3.1 Analysis of REM results and discussion

3.1.1 Mathematical modeling

According to the planning of experiments in Table 3, different process parameters combinations are assigned to the finite element model established above, and then the simulation results were included in "The Response" in Table 3. These results were used to establish empirical models.

Table 3 Experimental plan and FE Simulation results

No.	Processing parameters				Response variable		
	x_1 (L/D)	x_2 (μ_1)	x_3 (μ_2)	x_4 (υ)	φ (%)	ψ (%)	ξ (%)
1	3.425	0.03	0.12	0.4921	10.25	16.80	7.04
2	4.475	0.03	0.12	0.4921	9.70	17.05	7.38
3	3.425	0.09	0.12	0.4921	10.75	15.70	5.37
4	4.475	0.09	0.12	0.4921	10.00	16.15	5.73
5	3.425	0.03	0.24	0.4921	9.90	17.40	7.42
6	4.475	0.03	0.24	0.4921	9.55	17.50	7.73
7	3.425	0.09	0.24	0.4921	9.50	17.55	6.64
8	4.475	0.09	0.24	0.4921	9.00	17.90	6.73
9	3.425	0.03	0.12	0.4962	10.75	16.60	6.46
10	4.475	0.03	0.12	0.4962	10.40	16.75	6.58
11	3.425	0.09	0.12	0.4962	11.15	15.60	4.52
12	4.475	0.09	0.12	0.4962	10.70	16.05	5.10
13	3.425	0.03	0.24	0.4962	10.35	17.05	6.43
14	4.475	0.03	0.24	0.4962	10.25	17.10	6.39
15	3.425	0.09	0.24	0.4962	9.95	17.40	5.83
16	4.475	0.09	0.24	0.4962	10.05	17.05	5.25
17	2.9	0.06	0.18	0.4942	9.50	16.60	6.49

18	5	0.06	0.18	0.4942	9.60	17.60	6.21
19	3.95	0	0.18	0.4942	10.00	16.85	6.79
20	3.95	0.12	0.18	0.4942	9.90	16.70	5.46
21	3.95	0.06	0.06	0.4942	11.45	15.10	5.02
22	3.95	0.06	0.3	0.4942	9.95	17.35	6.49
23	3.95	0.06	0.18	0.49	9.45	17.40	7.12
24	3.95	0.06	0.18	0.4983	10.30	15.10	5.61
25	3.95	0.06	0.18	0.4942	10.00	17.25	6.61

The second-order model was used to fit the simulation results, and regression analysis was conducted by the least square method to determine the polynomial coefficients of the empirical functions between the three responses and the four process parameters.

The response model of the maximum thinning rate (φ) was obtained as:

$$\begin{aligned}\varphi = &-441.45782 - 37.47364x_1 - 102.48468x_2 - 114.75151x_3 \\ &+ 2050.61788x_4 - 0.99206x_1x_2 + 2.48016x_1x_3 \\ &+ 79.96299x_1x_4 - 105.90278x_2x_3 + 251.12345x_2x_4 \\ &+ 174.29950x_3x_4 - 0.33501x_1^2 + 8.51473x_2^2 \\ &+ 54.21202x_3^2 - 2305.65745x_4^2\end{aligned} \tag{7}$$

The response model of the maximum thickening rate (ψ) was obtained as:

$$\begin{aligned}\psi = &-12093.19003 + 24.30531x_1 - 62.16865x_2 + 292.02573x_3 \\ &+ 48861.06797x_4 + 1.38889x_1x_2 - 2.28175x_1x_3 \\ &- 48.14773x_1x_4 + 157.98611x_2x_3 + 69.38937x_2x_4 \\ &- 530.33307x_3x_4 + 0.011251x_1^2 - 86.83230x_2^2 \\ &- 59.90252x_3^2 - 49300.16868x_4^2\end{aligned} \tag{8}$$

The response model of maximum cross-section ovality (ξ) is obtained as:

$$\begin{aligned}\xi = &-2556.10446 + 31.86584x_1 - 2.15336x_2 + 467.93133x_3 \\ &+ 10160.17023x_4 - 1.09203x_1x_2 - 3.24452x_1x_3 \\ &- 60.50560x_1x_4 + 111.55489x_2x_3 - 36.19161x_2x_4 \\ &- 885.44772x_3x_4 - 0.16056x_1^2 - 113.60391x_2^2 \\ &- 53.50382x_3^2 - 10090.52354x_4^2\end{aligned} \tag{9}$$

3.1.2 Analysis of variance of response model

In order to check the fitness of regression model fitting the real data points, a statistical measure R^2 is introduced. And the closer the value of R^2 to unity, the better the fit between the empirical model and the actual data. F value is another evaluation, which is the ratio of the mean square obtained by regression to the mean square due to residual. For the F value, there is a critical value F_0, and P value represent the probability of $F < F_0$. Generally, the model is considered to be significant and the influence of the terms on the response is significant when $P < 0.05$.

Table 4 shows the results of ANOVA applied to the individual coefficients for the maximum thinning rate response model (Eq. 7). The model P value is 0.0002 less than 0.0500, and R^2 is 0.9432, which can imply that the model is significant. The significant terms in the maximum thinning rate response model include x_1, x_3, x_4, x_2x_3, and x_3^2, where x_1 and x_4 are the greatest significant items with P value less than 0.0001, therefor the following will introduce the impact of these two on wall thickness thinning.

Table 4 Analysis of variance (ANOVA) for maximum thinning rate φ

Source	Sum of squares	Degree of freedom	Mean square	*F* value	*P* value	Probability > *F*
Model	7.16	14	0.51	11.87	0.0002	Significant
x_1	0.32	1	0.32	7.40	0.0215	Significant
x_2	2.667E-003	1	2.667E-003	0.062	0.8086	
x_3	2.77	1	2.77	64.29	< 0.0001	Significant
x_4	1.83	1	1.83	42.52	< 0.0001	Significant
x_1x_2	3.906E-003	1	3.906E-003	0.091	0.7695	
x_1x_3	0.098	1	0.098	2.27	0.1631	
x_1x_4	0.12	1	0.12	2.75	0.1282	
x_2x_3	0.58	1	0.58	13.49	0.0043	Significant
x_2x_4	3.817E-003	1	3.817E-003	0.089	0.7721	
x_3x_4	7.355E-003	1	7.355E-003	0.17	0.6882	
x_1^2	0.096	1	0.096	2.22	0.1668	
x_2^2	6.598E-004	1	6.598E-004	0.015	0.9040	
x_3^2	0.43	1	0.43	9.93	0.0103	Significant
x_4^2	1.104E-003	1	1.104E-003	0.026	0.8760	
Residual	0.43	10	0.043			
Cor Total	7.59	24				
R^2=0.9432						

Table 5 shows the results of ANOVA applied to the individual coefficients for the maximum thickening rate response model (Eq. 8). The model P value is 0.0054 less than 0.0500, and R^2 is 0.8835, which can imply that the model is significant. The significant terms in the maximum thickening rate response model include x_3, x_4, x_4, and x_2x_3, where x_3 are the greatest significant items with P value less than 0.0001.

Table 5 Analysis of variance (ANOVA) for maximum thickening rate ψ

Source	Sum of squares	Degree of freedom	Mean square	*F* value	*P* value	Probability > *F*
Model	12.61	14	0.90	5.42	0.0054	Significant
x_1	0.50	1	0.50	3.00	0.1138	
x_2	0.41	1	0.41	2.49	0.1457	
x_3	6.79	1	6.79	40.84	< 0.0001	Significant
x_4	2.10	1	2.10	12.65	0.0052	Significant
x_1x_2	7.656E-003	1	7.656E-003	0.046	0.8343	
x_1x_3	0.083	1	0.083	0.50	0.4967	
x_1x_4	0.043	1	0.043	0.26	0.6221	
x_2x_3	1.29	1	1.29	7.79	0.0191	Significant
x_2x_4	2.914E-004	1	2.914E-004	1.754E-003	0.9674	
x_3x_4	0.068	1	0.068	0.41	0.5365	
x_1^2	1.080E-004	1	1.080E-004	6.502E-004	0.9802	
x_2^2	0.069	1	0.069	0.41	0.5349	
x_3^2	0.52	1	0.52	3.14	0.1066	
x_4^2	0.50	1	0.50	3.04	0.1120	
Residual	1.66	10	0.17			
Cor Total	14.27	24				
R^2=0.8835						

Table 6 shows the results of ANOVA for the maximum cross-section ovality response model (Eq. 9). The P value of the model is 0.0003, which is much less than 0.05, and R^2 is 0.9386, which means that the model is significant. Terms x_2, x_3, x_4 and x_2x_3 have significant influence on maximum cross-section ovality. And x_2 and x_4 are the greatest significant items with P value less than 0.0001.

Table 6 Analysis of variance (ANOVA) for maximum cross-section ovality ξ

Source	Sum of squares	Degree of freedom	Mean square	*F* value	*P* value	Probability > *F*
Model	15.39	14	1.10	10.91	0.0003	Significant
x_1	0.016	1	0.016	0.16	0.6994	
x_2	6.92	1	6.92	68.72	< 0.0001	Significant
x_3	2.16	1	2.16	21.47	0.0009	Significant
x_4	4.61	1	4.61	45.73	< 0.0001	Significant

x_1x_2	4.733E-003	1	4.733E-003	0.047	0.8328	
x_1x_3	0.17	1	0.17	1.66	0.2268	
x_1x_4	0.068	1	0.068	0.67	0.4309	
x_2x_3	0.65	1	0.65	6.40	0.0298	Significant
x_2x_4	7.928E-005	1	7.928E-005	7.870E-004	0.9782	
x_3x_4	0.19	1	0.19	1.88	0.1999	
x_1^2	0.022	1	0.022	0.22	0.6503	
x_2^2	0.12	1	0.12	1.17	0.3056	
x_3^2	0.42	1	0.42	4.14	0.0693	
x_4^2	0.021	1	0.021	0.21	0.6567	
Residual	1.01	10	0.10			
Cor Total	16.40	24				
			R^2=0.9386			

It can be seen that the x_3 i.e., the friction coefficient between the tube and the polyurethane mandrel has the greatest impact both on the thinning rate and the thickening rate of the bent tube wall thickness. x_3 mainly affects the friction force between the polyurethane mandrel and the tube, thereby affecting the tangential force of the bent tube. While the thinning or the thickening of the wall thickness of the tube in the bending process is mainly due to the external tangential force, so the x_3 is a significant term in the maximum thinning rate response model as well as maximum thickening rate response model.

The value of Poisson's ratio directly affects the compressibility of polyurethane mandrel. Under the condition of applying the same force, different Poisson's ratio polyurethanes will have different contact pressure response with the tube due to different compressibility when expanding in the sealed tube. The support internal pressure provided by polyurethane mandrel not only affects the friction force, but also greatly affects the deformation of the tube cross-section. Therefore, x_4 is the greatest significant term in the maximum thinning rate response model and the maximum cross-section ovality response model.

Also noted that x_2 is another greatest significant item with P-value less than 0.0001 in the maximum cross-section ovality response model. The reason is that the coefficient of friction between die and tube will affect the flow of tube material in the die during bending process, which results in different cross-section ovality responses.

3.1.3 Response surface analysis

The 3D response surface plots were drawn to visualize the influence of the variables on the responses. There are 4 process parameters in the study, but only two of the process parameters can be shown in a 3D response surface diagram. So, the four process parameters are divided into two categories, friction coefficient (includes x_2 and x_3) and parameters of polyurethane (includes x_1 and x_4). x_2 and x_3 was used as a group to plot a 3D response surface ($x_1 = 4,\ x_4 = 0.4983$). x_1 and x_4 was used as another group to construct a 3D response surface ($x_2 = 0.08,\ x_3 = 0.15$).

Fig. 7 to Fig. 9 show the influence of x_2 (the coefficient of friction between the tube and die) and x_3 (the coefficient of friction between the tube and polyurethane) on φ (the maximum thinning rate), ψ (the maximum thickening rate), and ξ (the maximum cross-section ovality), respectively. And Fig. 10 to Fig. 12 show the influence of x_1 (the relative length of the mandrel) and x_4 (the Poisson's ratio of polyurethane) on φ, ψ, and ξ, respectively.

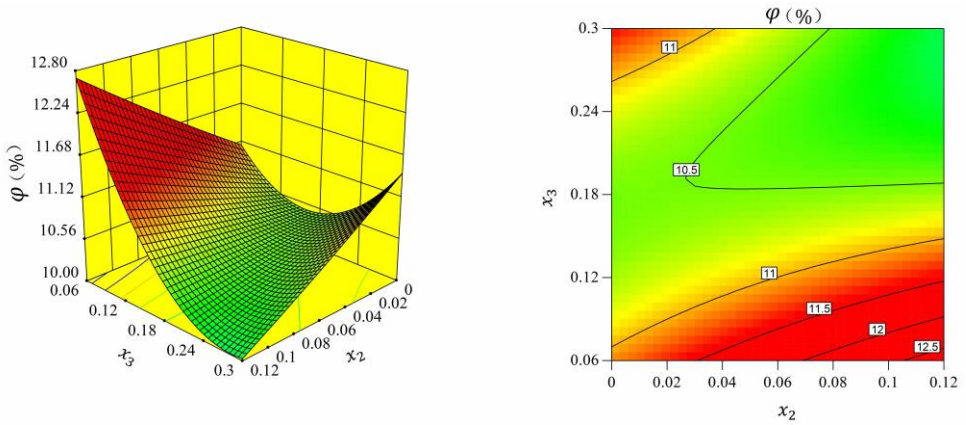

(a) (b)

Fig. 7 Response surface and contour plot for maximum thinning rate φ when $x_1 = 4$ and $x_4 = 0.4983$ (a) 3D response surface (b) Contour plot

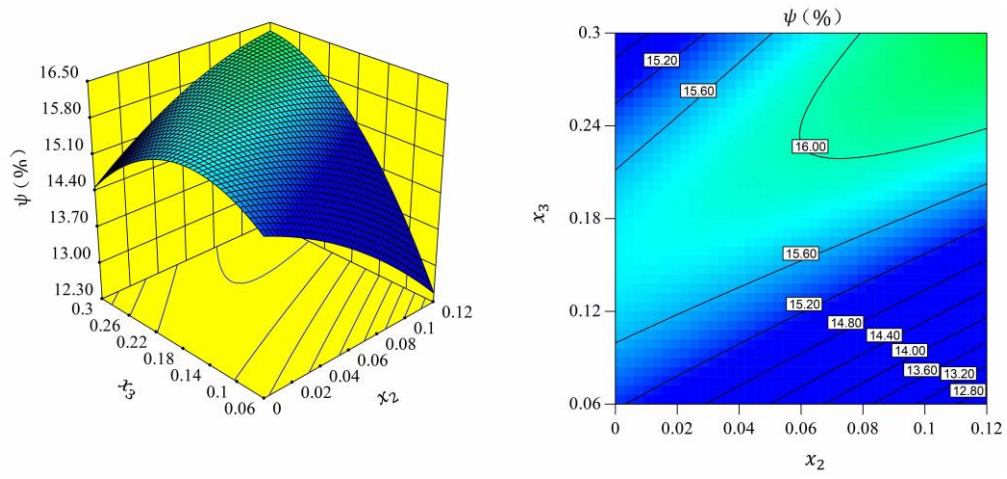

(a) (b)

Fig. 8 Response surface and contour plot for maximum thickening rate ψ when $x_1 = 4$ and $x_4 = 0.4983$ (a) 3D response surface (b) Contour plot

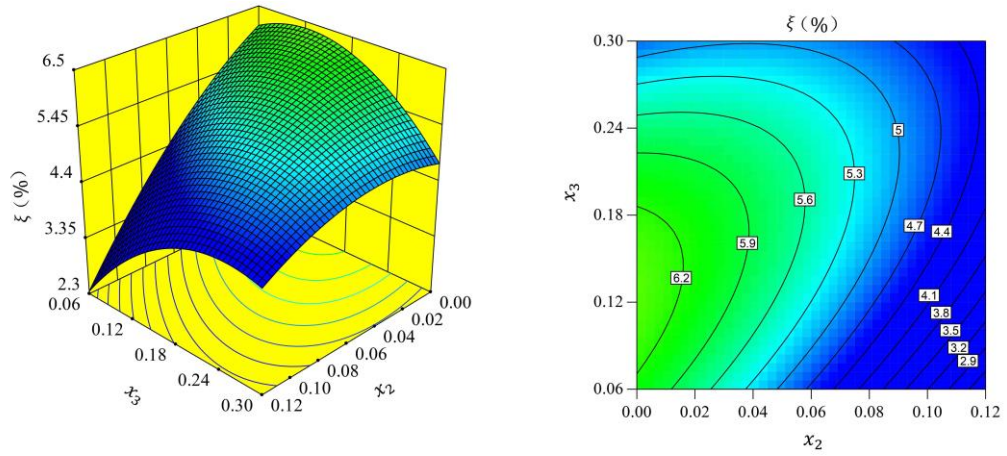

(a) (b)

Fig. 9 Response surface and contour plot for maximum cross-section ovality ξ when $x_1 = 4$ and $x_4 = 0.4983$ (a) 3D response surface (b) Contour plot

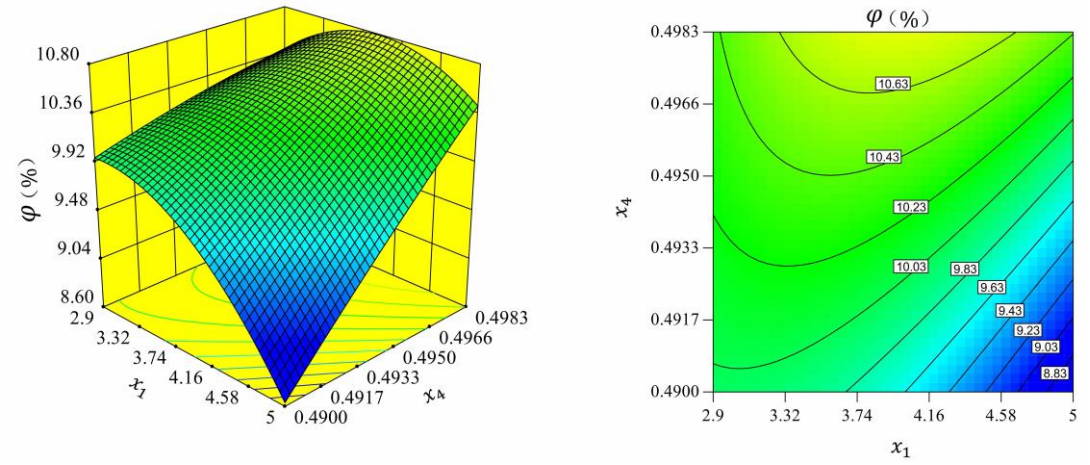

(a) (b)

Fig. 10 Response surface and contour plot for maximum thinning rate φ when $x_2 = 0.08$ and $x_3 = 0.15$ (a) 3D response surface (b) Contour plot

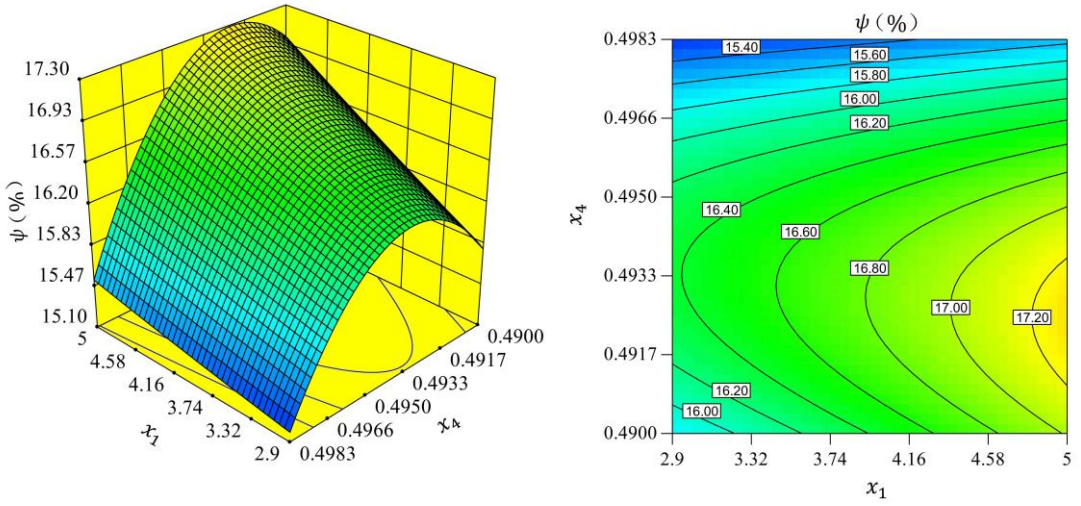

(a) (b)

Fig. 11 Response surface and contour plot for maximum thickening rate ψ when $x_2 = 0.08$ and $x_3 = 0.15$ (a) 3D response surface (b) Contour plot

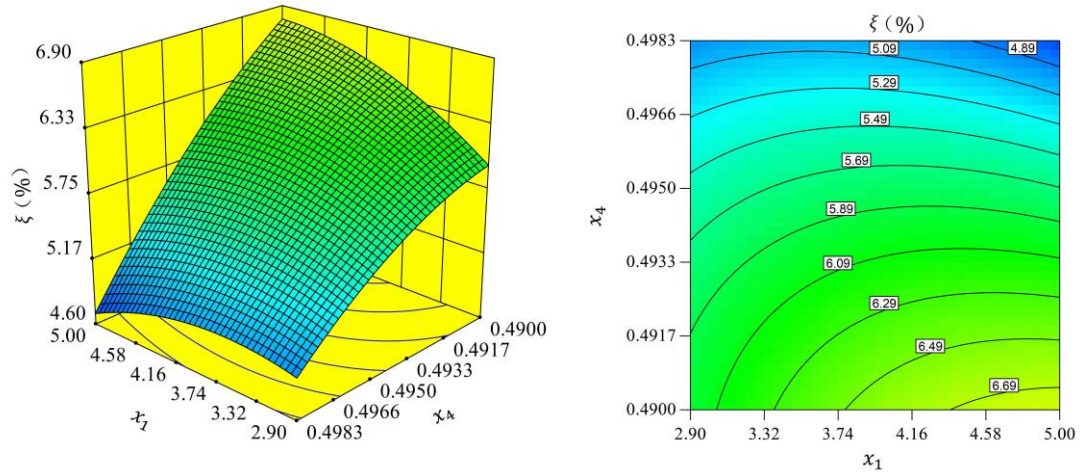

(a) (b)

Fig. 12 Response surface and contour plot for maximum cross-section ovality ξ when $x_2 = 0.08$ and $x_3 = 0.15$ (a) 3D response surface (b) Contour plot

It can be found that the forming quality of the bent tube is often influenced by the multiple instabilities and multi-factor coupling effects. There may be causing a change of one forming parameter on the law of forming quality of the bent tube when a change of another forming parameter. A typical result which is the influence of x_2 and x_3 on φ (Fig. 7) illustrates this deeply. If x_3 is small, the maximum thinning rate increases linearly with the increase of x_2, but when x_3 is greater than a certain critical value, the maximum thinning rate will decrease linearly with the increase of x_2.

A comparison between Figure 7 and Figure 8 can be found that the effect of x_2 (the coefficient of friction between the tube and die) on the maximum thickening rate and maximum thinning rate is opposite. For example, if x_3 is set to 0.06, increasing

x_2 will reduce the maximum thickening rate, but inevitably increase the maximum thinning rate. That is, by adjusting x_2 to mitigate one forming defect, it will exacerbate another forming defect.

The forming quality is greatly influenced by the Poisson's ratio of polyurethane. The higher Poisson's ratio of the polyurethane mandrel is helpful to reduce cross-section ovality of the bent tube but increase the maximum thinning rate. Therefore, the choice of polyurethane material is also a very important issue in the push-bending process with polyurethane mandrel.

3.2 Analysis of multi-objective process optimization and experiment results

As mentioned above, the bending forming quality of tube is affected by the interaction of multiple forming parameters, and it is not possible to reduce all forming defects by adjusting only one of the parameters. Therefore, it is useful to use the results of the response surface analysis to build multi-objective process windows.

In this study, the product process optimization window with critical maximum thinning rate of 20%, critical maximum thickening rate of 17%, and the critical maximum ovality of 5% were used as the qualified standard according to the industrial standard of QJ 919A-1998. As shown in Figure 13, the 0Cr18Ni9 qualified stainless-steel elbow with an outer diameter of 144 mm, a wall thickness of 2 mm, a bending radius of 280 mm, and a bending Angle of 70 ° can be obtained by the combination of process parameters in the yellow area in the figure.

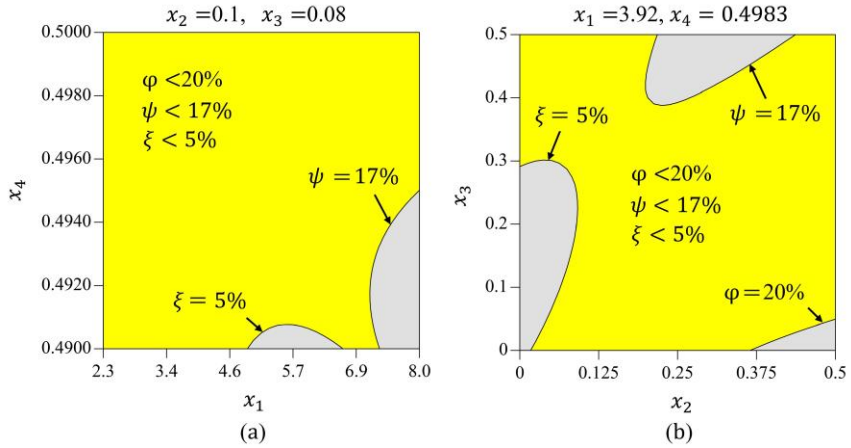

Fig. 13 Process optimization window for the tube push-bending process with polyurethane mandrel

The bending test was carried out by using the process parameters of the qualified area in the process optimization window. The relative length of the polyurethane mandrel used in the experiments is 3.92; The Poisson's ratio of polyurethane is 0.4983; Engine oil is used to lubricate the inner and outer walls of the tube blank, the die cavity and the outer surface of the polyurethane mandrel. Three experiments were conducted using the same parameters.

The elbow obtained from the above experiment is shown in Figure 14. The wall thickness distribution and section diameter distribution of the bend tube are given to indicate the forming quality of the bent tube formed from this method (Figure 15). Hence the maximum thinning rate φ, the maximum thickening rate ψ and the maximum cross-section ovality ξ of the obtained elbow were calculated according to formula 1 to formula 3. Table 7 shows the experimental results of φ, ψ and ξ. The results show that the product was formed with high quality using push-bending process with polyurethane mandrel, and the reliability of forming process optimization window based on response surface analysis was also shown.

Fig. 14 Bent tubes formed with optimized process parameters

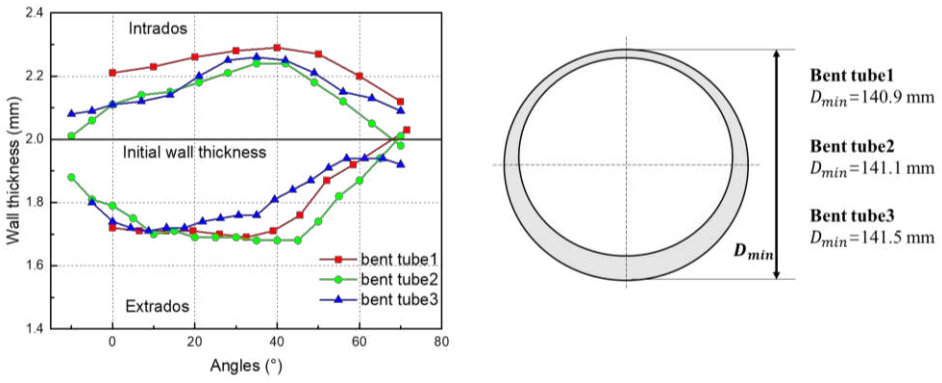

Fig. 15 Wall thickness and cross-section diameter of thin-walled bending tubes

Table 7 Experimental results of φ, ψ and ξ of bent tubes

Items	Maximum thinning rate $\boldsymbol{\varphi}$ (%)	Maximum thickening rate $\boldsymbol{\psi}$ (%)	Maximum cross-section ovality $\boldsymbol{\xi}$ (%)
Maximum allowable value	20	17	5
Bent tube 1	15.5	14.5	2.1
Bent tube 2	16	12	2
Bent tube 3	14.5	13	1.7

4 Conclusions

CCD-RSM was used to analyze tube push-bending process with polyurethane mandrel based on the FEM. The main conclusions are as follows:

(1) The empirical functions between the three forming quality indicators and four process parameters were developed.

(2) The ANOVA shows that the friction coefficient between the tube and the polyurethane mandrel has the greatest impact both on the thinning rate and the thickening rate of the bent tube wall thickness; The value of Poisson's ratio is the greatest significant term in the maximum thinning rate response model and the maximum cross-section ovality response model; The coefficient of friction between die and tube is another greatest significant item in the maximum cross-section ovality response model.

(3) The bending forming quality of tube is affected by the interaction of multiple forming parameters, and it is not possible to reduce all forming defects by adjusting only one of the parameters.

(4) The process optimization window with critical φ of 20%, critical ψ of 17%, and the critical ξ of 5% was used as the qualified standard. And the qualified bent tubes were formed experimentally by following the established process window. The forming process optimization window based on response surface analysis has high reliability and is suitable for industrial applications.

Nomenclature

D = Initial outer diameter of tube

t_0 = Initial wall thickness of tube

R = centerline radius of bent tube

L = center axis length of polyurethane mandrel

L/D (x_1) = the relative length of the mandrel

μ_1 (x_2)= the friction coefficient between die and tube

μ_2 (x_3)= the friction coefficient between polyurethane and tube

υ (x_4) = Poisson's ratio of polyurethane

φ = the maximum thinning rate of the bent tube

ψ = the maximum thickening rate of the bent tube

ξ = the maximum cross-section ovality of the bent tube

t_{min}= the minimum wall thickness of bent tube

t_{max}= the maximum wall thickness of bent tube

D_{min}= the minimum outer diameter of bent tube

E = the elastic modulus of polyurethane

E_s = the compression modulus of polyurethane

y = the response in RSM

x_i = the process parameter i in RSM

ϵ = the experimental random error in RSM

k = the number of process parameters in RSM

R^2 = a statistical measure in RSM

F = the ratio of the mean square obtained by regression to the mean square due to residual

F_0 = the critical value of F

P = the probability of $F < F_0$

Authors' contributions

Wenlong Xie: Methodology, Investigation, Software, Validation and Writing.

Weihao Jiang: Methodology, Investigation, Software.

Yunfeng Wu: Investigation, Conceptualization.

Hong-wu Song: Methodology, Investigation, Conceptualization, Funding acquisition, Writing-Reviewing & Editing.

Siying Deng: Investigation, Writing-Reviewing & Editing.

Lucian Lăzărescu: Methodology, Software, Writing-Reviewing & Editing

Shi-Hong Zhang: Conceptualization, Funding acquisition, Supervision, Writing-Reviewing & Editing.

Dorel Banabic: Writing-Reviewing & Editing

Funding

This study was funded by the National Natural Science Foundation of China (Grant No. 51875547).

Data availability

All the data and materials in this study are available upon reasonable request.

Compliance with ethical standards

Ethical approval

The authors claim that none of the contents in this manuscript has been published or considered for publication elsewhere. Besides, the research contents of the article do not violate ethics.

Consent to participate

For this type of study, consent to participate was not required.

Consent to publish

For this type of study, consent to publish was not required.

Competing interests

The authors declare that they have no conflict of interest.

References

[1] Yang H, Li H, Zhan M. (2010) Friction role in bending behaviors of thin-walled tube in rotary-draw-bending under small bending radii. J Mater Process Technol 210(15), 2273-2284. https://doi.org/10.1016/j.jmatprotec.2010.08.021

[2] He Y, Heng L, Zhang Z, et al (2012) Advances and trends on tube bending forming technologies. Chin J Aeronaut 25(1), 1-12. https://doi.org/10.1016/S1000-9361(11)60356-7

[3] Liu N, Yang H, Li H, et al (2015) An imperfection-based perturbation method for plastic wrinkling prediction in tube bending under multi-die constraints. Int J Mech Sci 98: 178-194. https://doi.org/10.1016/j.ijmecsci.2015.03.023

[4] Yang J, Jeon B, Oh S I (2001) The tube bending technology of a hydroforming process for an automotive part. J Mater Process Technol 111(1-3), 175-181. https://doi.org/10.1016/S0924-0136(01)00505-2

[5] Liu H, Zhang S H, Song H W, et al (2019) 3D FEM-DEM coupling analysis for granular-media-based thin-wall elbow tube push-bending process. Int J Mater Form 12(6), 985-994. https://doi.org/10.1007/s12289-019-01473-8

[6] Li H, Yang H, Yan J, et al (2009) Numerical study on deformation behaviors of thin-walled tube NC bending with large diameter and small bending radius. Comput Mater Sci 45(4), 921-934. https://doi.org/10.1016/j.commatsci.2008.12.018

[7] Teng B, Lan H, Gang L I U, et al (2012) Wrinkling behavior of hydro bending of carbon steel/Al-alloy bi-layered tubes. T Nonferr Metal Soc 22, s560-s565.https://doi.org/10.1016/S1003-6326(12)61761-0

[8] Zeng Y, Li Z (2002) Experimental research on the tube push-bending process. J Mater Process Technol 122(2-3), 237-240. https://doi.org/10.1016/S0924-0136(02)00027-4

[9] Nguyen D T, Nguyen D T, Kim Y S (2015) Improving formability of tube bending for a copper material using finite element simulation. J Mech Sci Technol 29(10), 4205-4211. https://doi.org/10.1007/s12206-015-0915-2

[10] Safdarian, R (2019) Investigation of tube fracture in the rotary draw bending process using experimental and numerical methods. Int J Mater Form 1-24. https://doi.org/10.1007/s12289-019-01484-5

[11] Xu X, Wu K, Wu Y, et al (2019) Push-bending method development of thin-walled tube with relative bending radius of 1 using sectional elastomers as mandrel. Int J Adv Manuf Technol 105(1), 995-1008. https://doi.org/10.1007/s00170-019-04266-0

[12] Xu X, Fan Y, Wu Y, et al (2020) A novel differential lubrication method for push-bending of L-shaped thin-walled tube with 1D bending radius. Int J Mater Form 1-11. https://doi.org/10.1007/s12289-020-01563-y

[13] Zhu Y, Liu Y, He Y (2012) Sensitivity of springback and section deformation to process parameters in rotary draw bending of thin-walled rectangular H96 brass tube. T Nonferr Metal Soc 22(9): 2233-2240. https://doi.org/10.1016/S1003-6326(11)61454-4

[14] Li H, Yang H, Zhang Z Y, et al (2014) Multiple instability-constrained tube bending limits. J Mater Process Technol 214(2): 445-455. https://doi.org/10.1016/j.jmatprotec.2013.09.027

[15] Lăzărescu L (2010) FE simulation and response surface methodology for optimization of tube bending process. The Annals of" Dunarea de Jos" University of Galati, Fascicle V, Technologies in machine building 28(2): 93-100. https://www.gup.ugal.ro/ugaljournals/index.php/tmb/article/view/1843

[16] Wang L, Lee T C (2005) Controlled strain path forming process with space variant blank holder force using RSM method. J Mater Process Technol 167(2-3): 447-455. https://doi.org/10.1016/j.jmatprotec.2005.06.017

[17] Lepadatu D, Hambli R, Kobi A, et al (2005) Optimisation of springback in bending processes using FEM simulation and response surface method. Int J Adv Manuf Technol 27(1): 40-47.

https://doi.org/10.1007/s00170-004-2146-z

[18] Liu Y, Wang J, Wang D (2017) Numerical optimization on hot forging process of connecting rods based on RSA with experimental verification. Int J Adv Manuf Technol 90(9): 3129-3135. https://doi.org/10.1007/s00170-016-9635-8

[19] Jiang W, Xie W, Song H, et al (2020) A modified thin-walled tube push-bending process with polyurethane mandrel. Int J Adv Manuf Technol 106(5):2509-2521. https://doi.org/10.1007/s00170-019-04827-3

[20] Chu T H , Fuh K H , Yeh W C (2011). Experimental Optimization of Deep Drawing Using Response Surface Methodology. Appl Mech Mater 121–126, 1495–1499. https://doi.org/10.4028/www.scientific.net/amm.121-126.1495

Figures

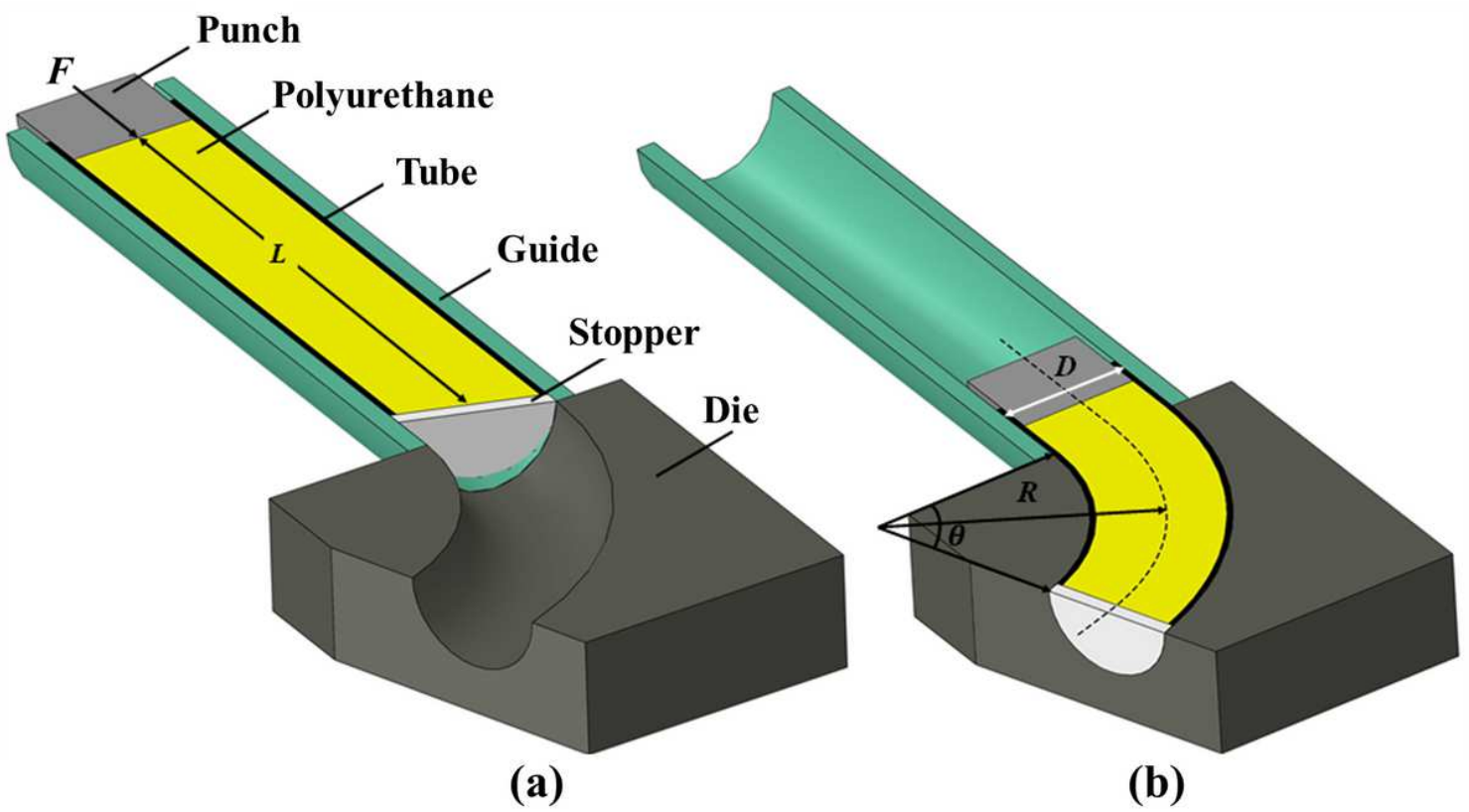

Figure 1

Schematics of the tube push-bending process with polyurethane mandrel (a) before bending (b) after bending [19].

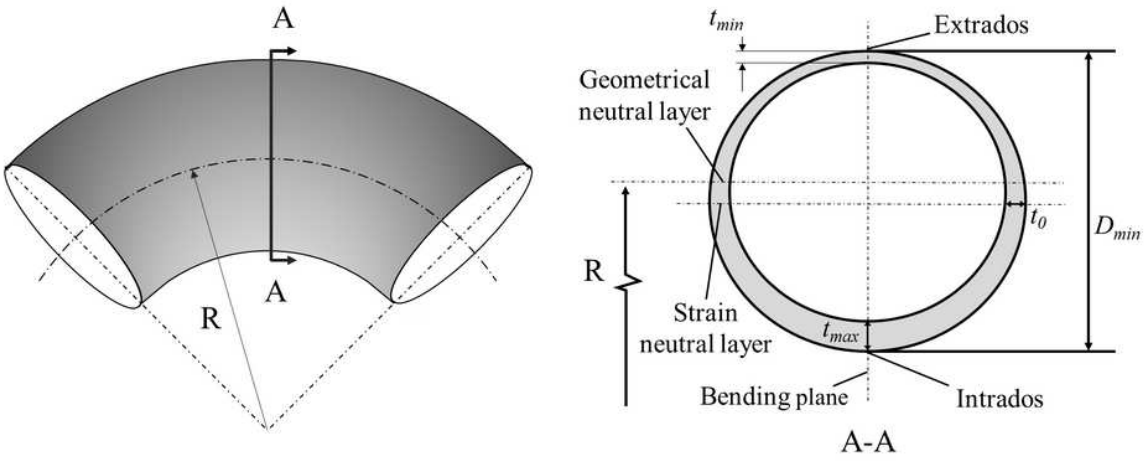

Figure 2

Schematic diagram of tube cross-section after bending

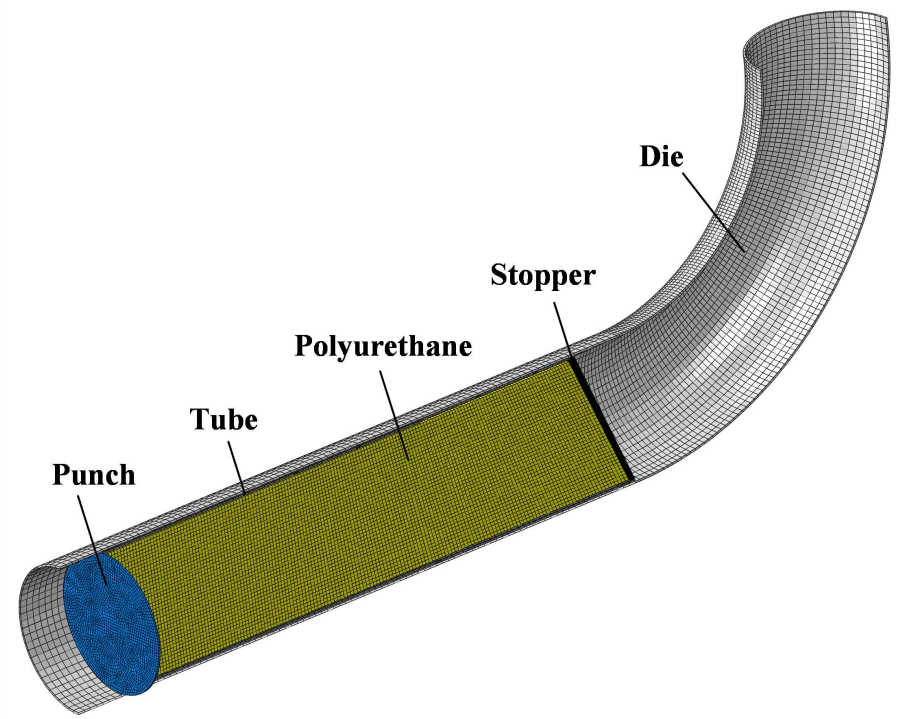

Figure 3

Schematics of FE model.

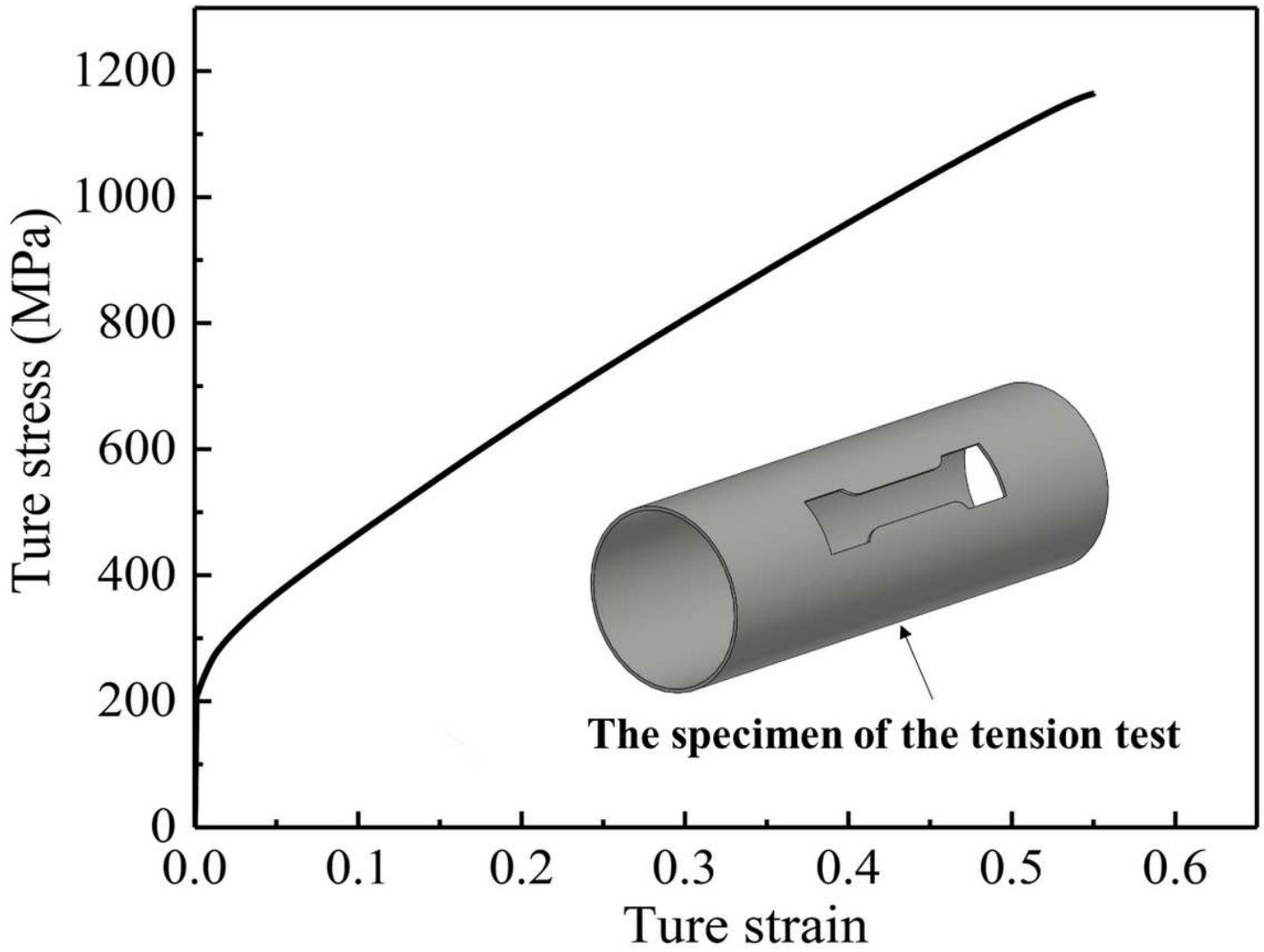

Figure 4

True stress-strain curve of 0Cr18Ni9 tubular blank

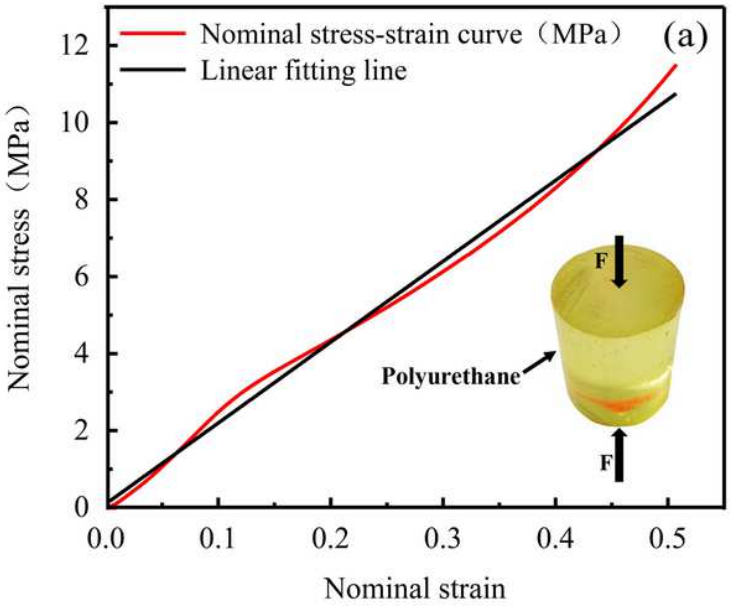

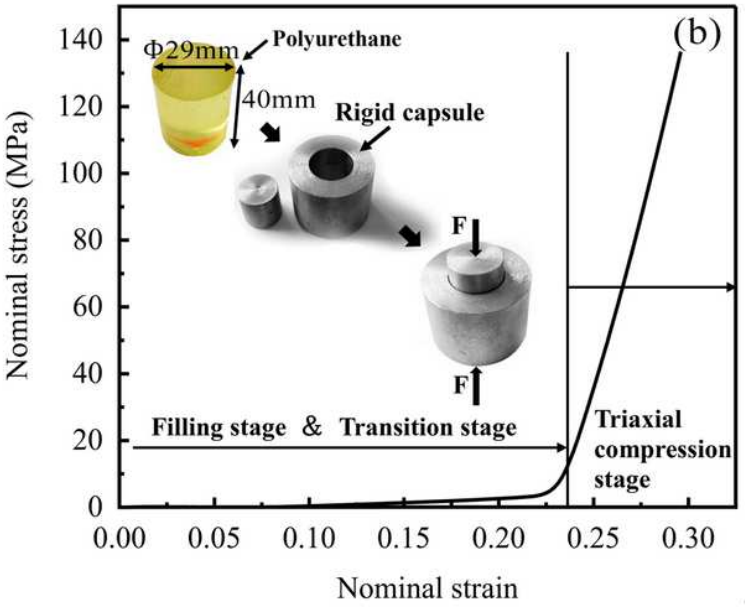

Figure 5

Nominal stress-strain curve of polyurethane (a) Uniaxial compression (b) Triaxial compression [19].

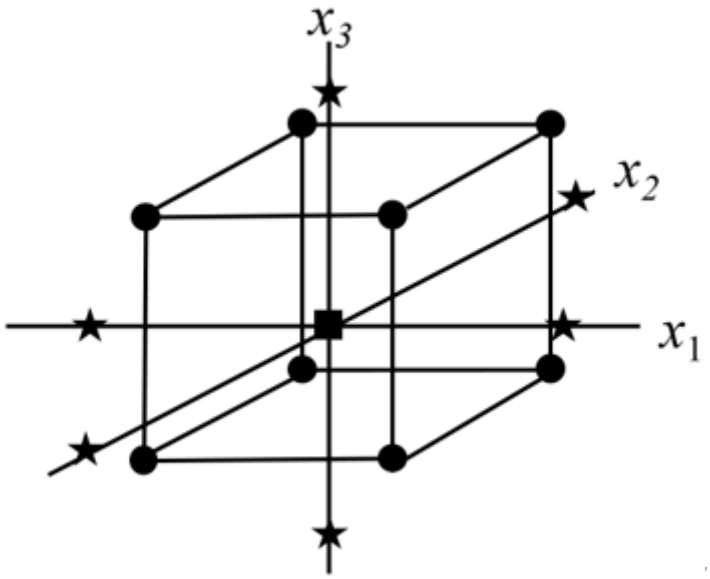

Figure 6

Central composite design for three factors

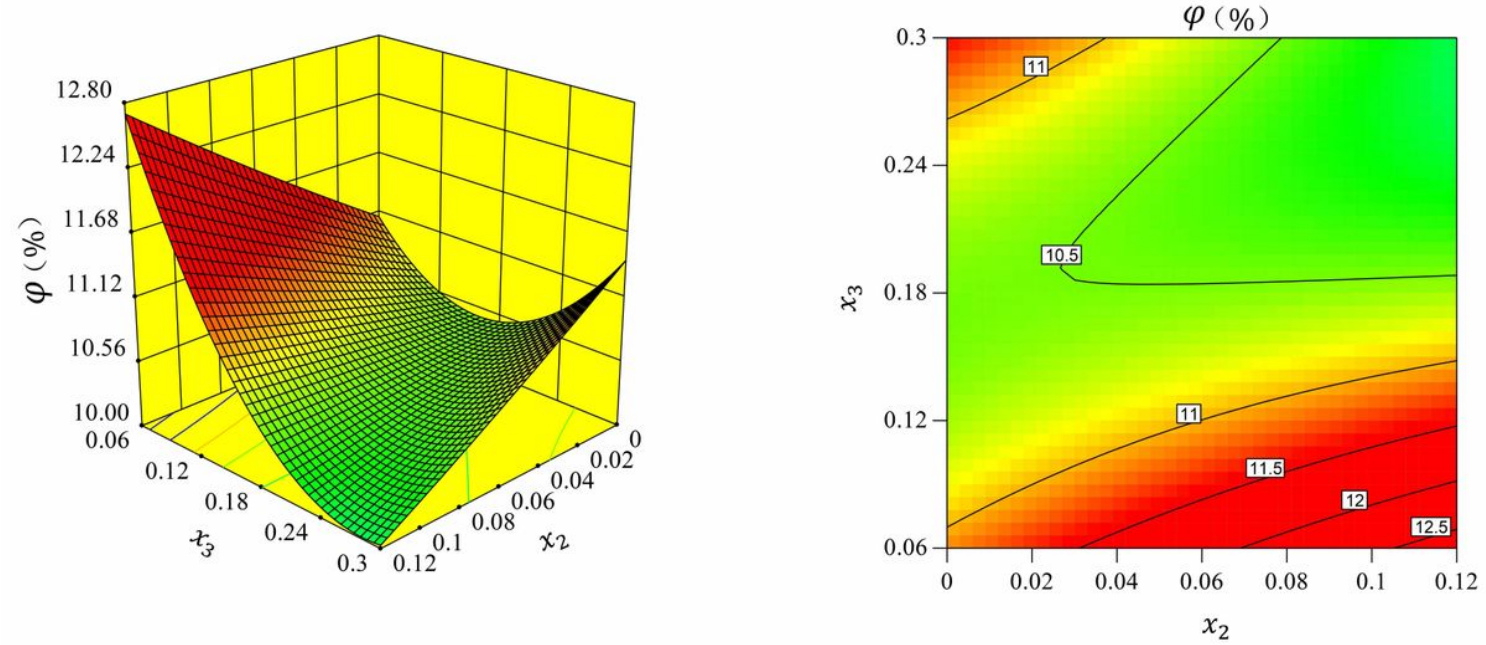

Figure 7

Response surface and contour plot for maximum thinning rate φ when x1=4 and x4=0.4983 (a) 3D response surface (b) Contour plot

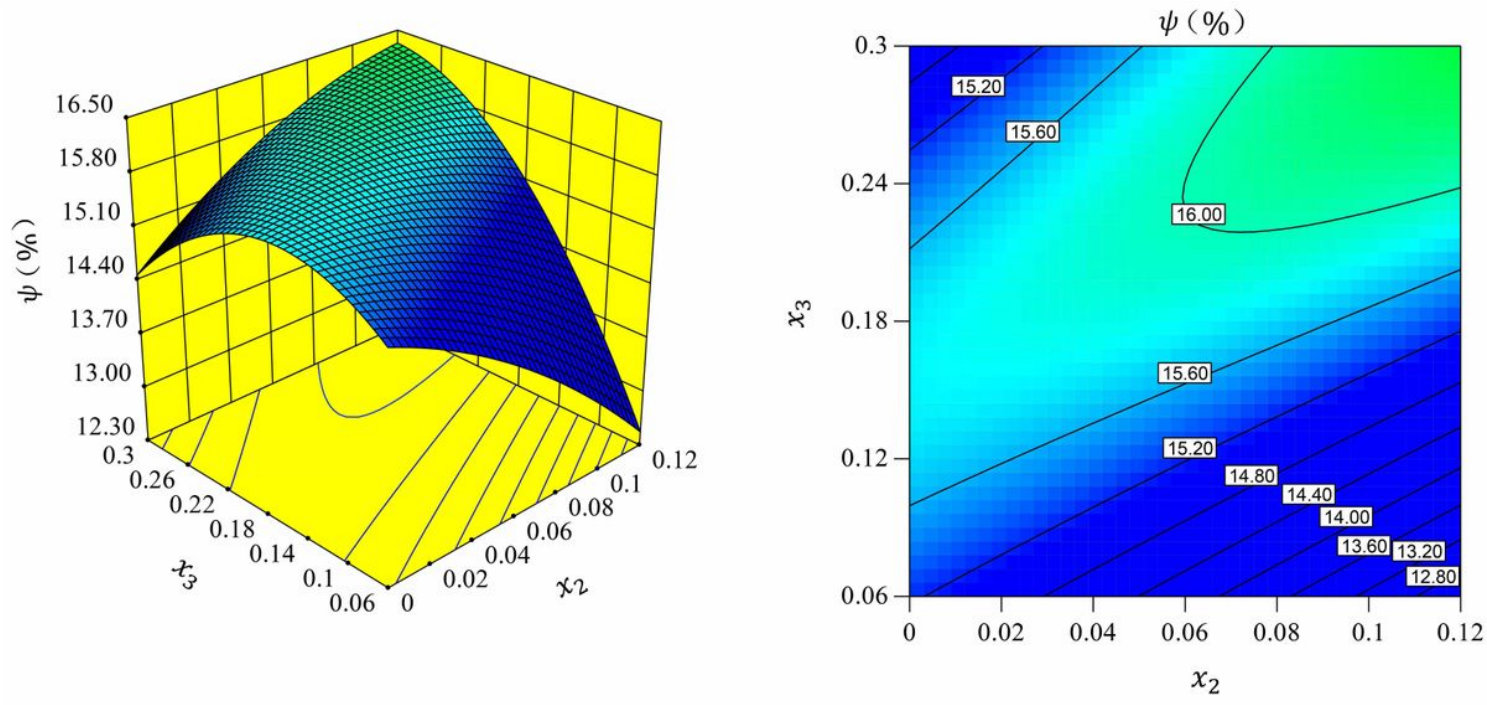

Figure 8

Response surface and contour plot for maximum thickening rate ψ when x1=4 and x4=0.4983 (a) 3D response surface (b) Contour plot

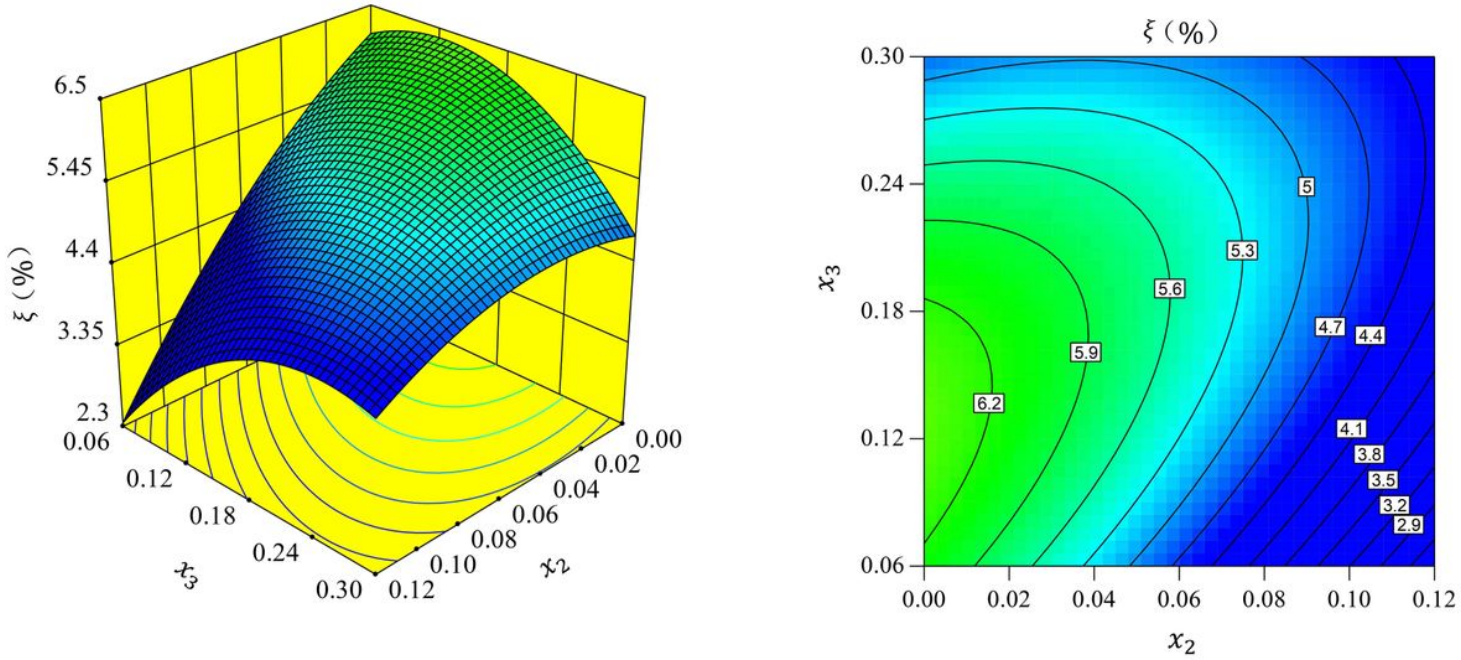

Figure 9

Response surface and contour plot for maximum cross-section ovality ξ when x1=4 and x4=0.4983 (a) 3D response surface (b) Contour plot

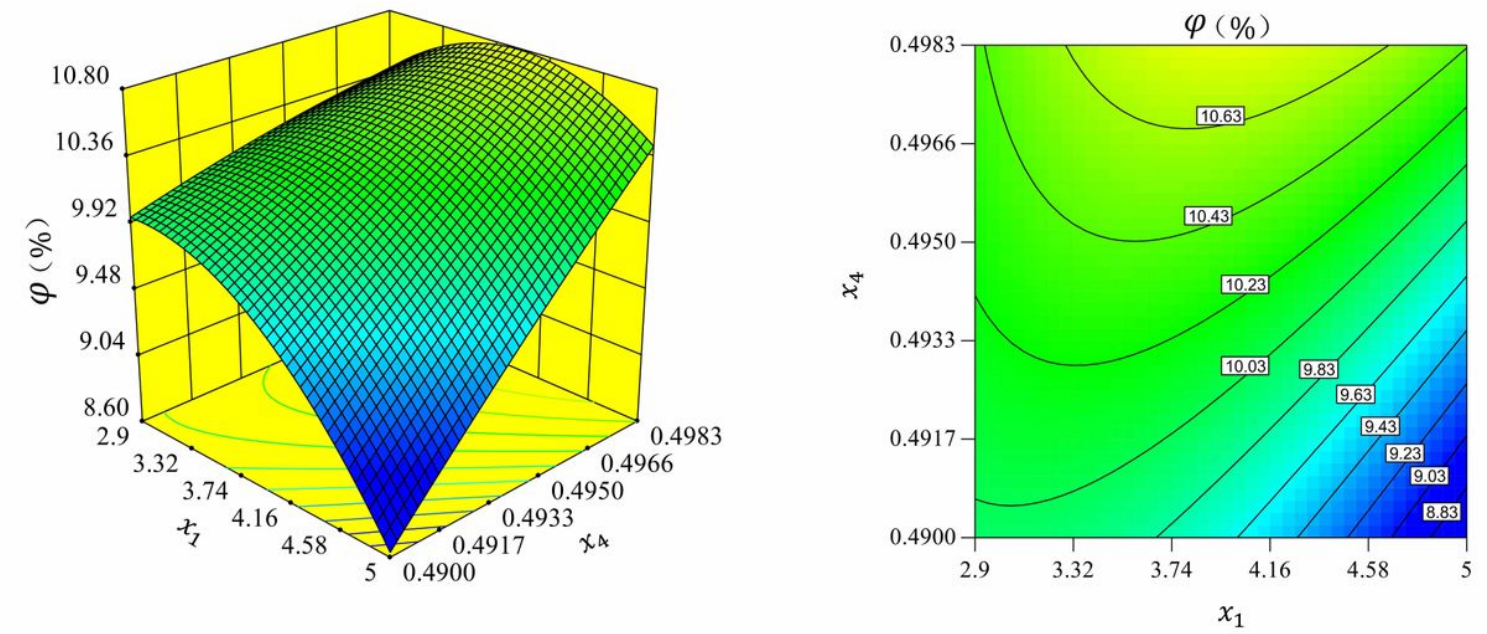

Figure 10

Response surface and contour plot for maximum thinning rate φ when x2=0.08 and x3=0.15 (a) 3D response surface (b) Contour plot

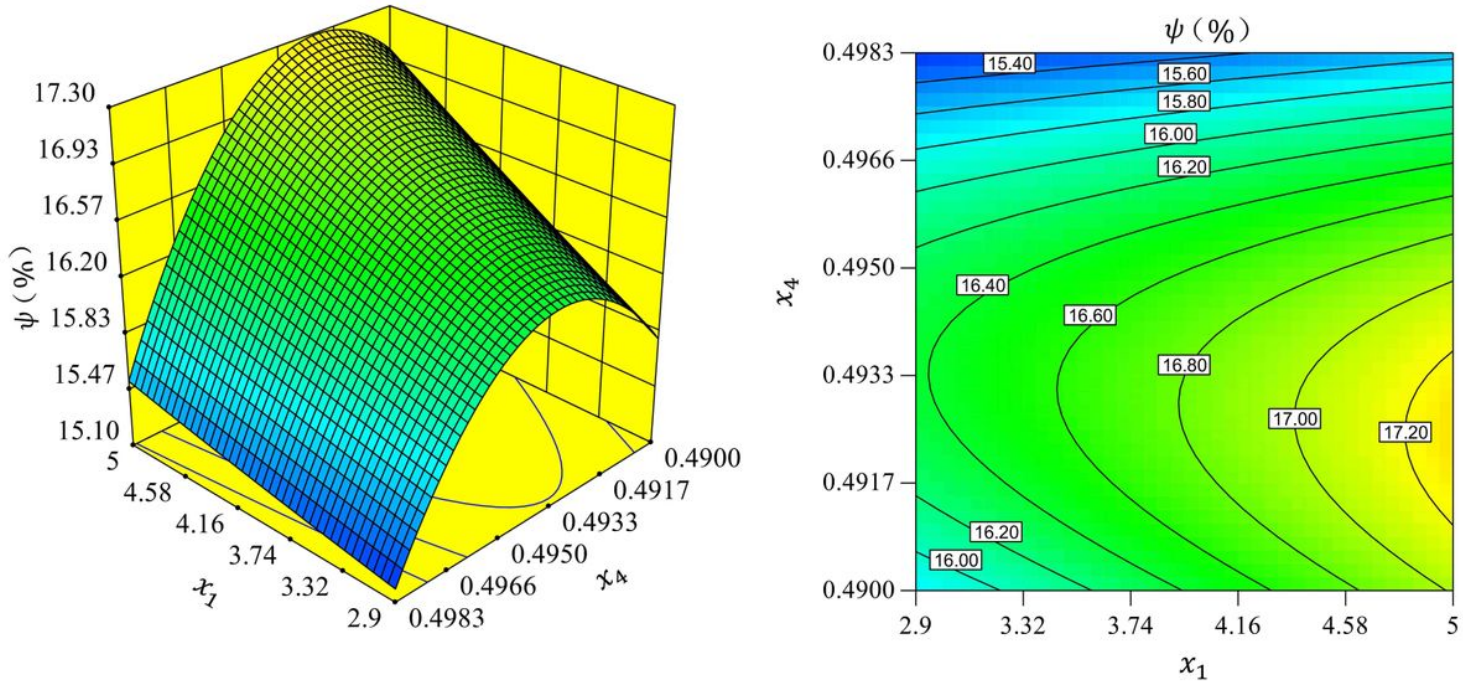

Figure 11

Response surface and contour plot for maximum thickening rate ψ when x2=0.08 and x3=0.15 (a) 3D response surface (b) Contour plot

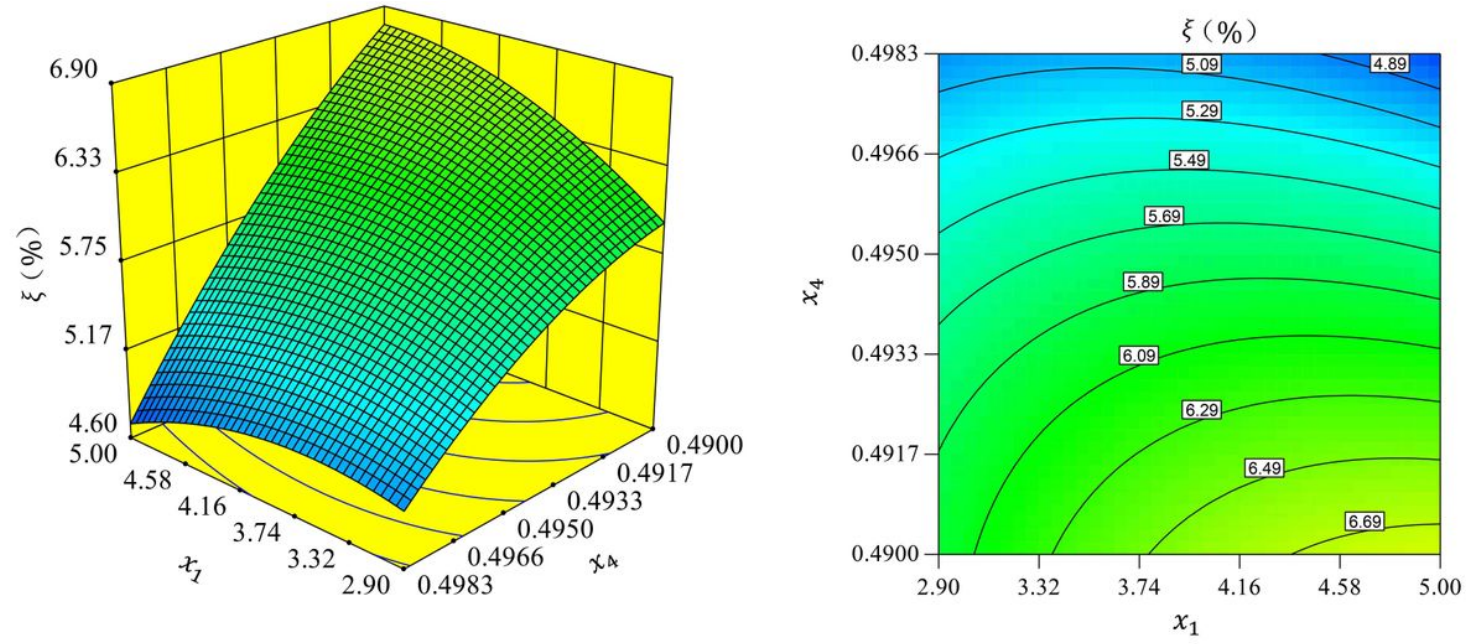

Figure 12

Response surface and contour plot for maximum cross-section ovality ξ when x2=0.08 and x3=0.15 (a) 3D response surface (b) Contour plot

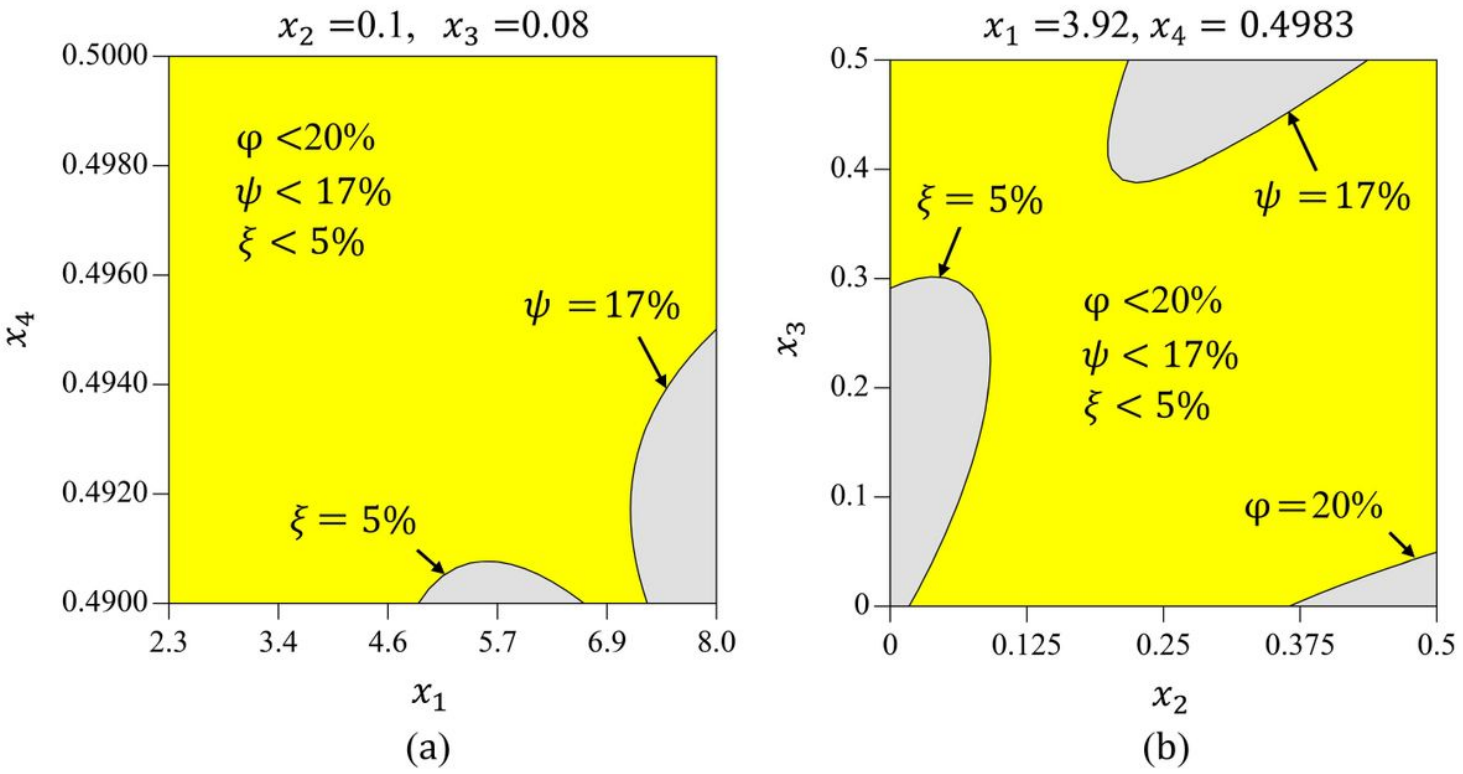

Figure 13

Process optimization window for the tube push-bending process with polyurethane mandrel

Figure 14

Bent tubes formed with optimized process parameters

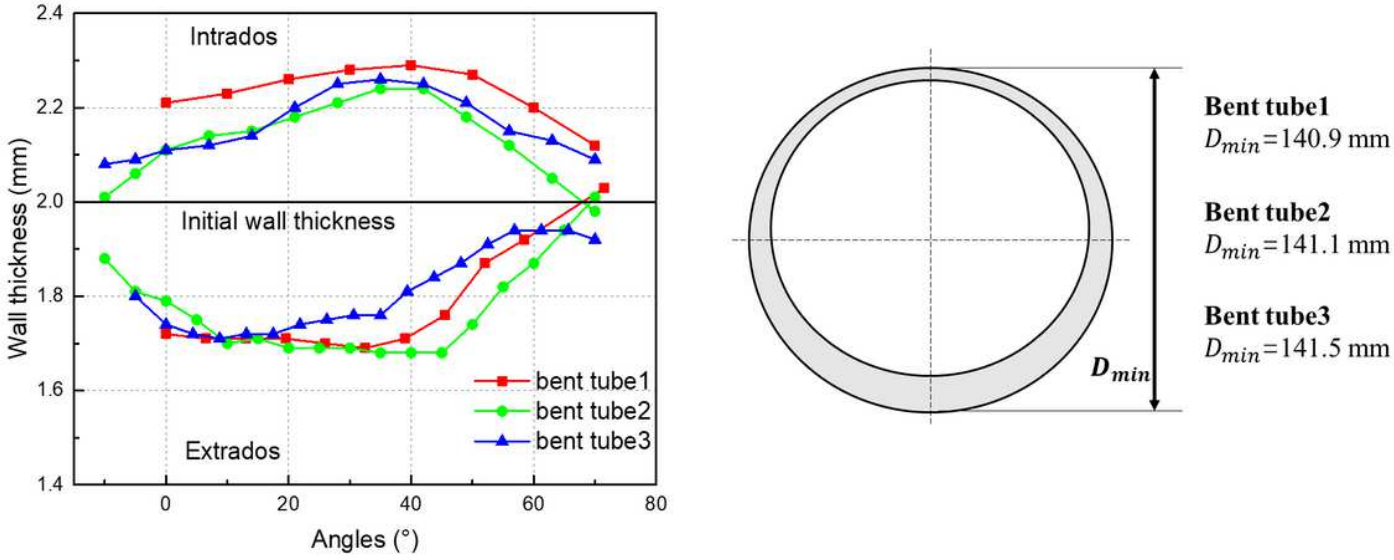

Figure 15

Wall thickness and cross-section diameter of thin-walled bending tubes